Int. J. Heat Mass Transfer. Vol. 36, No. 14, pp. 3497–3508, 1993
Printed in Great Britain

0017–9310/93 $6.00 + 0.00

Heat transfer enhancement in a ribbed duct using vortex generators

T. A. MYRUM, X. QIU and S. ACHARYA
Mechanical Engineering Department, Louisiana State University, Baton Rouge, LA 70803, U.S.A.

(*Received* 10 *July* 1992 *and in final form* 1 *February* 1993)

Abstract—Local and average Nusselt number and overall pressure drop results were obtained experimentally for an air flow ($Re \approx 3450$) in a ribbed duct with vortex generators (circular rods) placed immediately above or just downstream of select rib elements. The larger diameter generators ($d/h = 1.0$) for the two dimensionless rib pitches studied ($P/h = 38.4$ and 19.2) resulted in average Nusselt number, $\overline{Nu}$, increases as large as 21 and 12%, respectively, and entropy generation per unit heated length, S', decreases as large as 27 and 9%, respectively. The smaller diameter generators ($d/h = 0.50$) generally had no effect on either $\overline{Nu}$ or S'.

INTRODUCTION

RIB-LIKE geometries arise in a number of applications, such as heat exchangers, arrays of electronic components, etc. Therefore, there is a need for improved heat transfer performance in ribbed ducts. To this end, Hung and Lin [1] positioned a two-dimensional turbulence promoter on the vertical wall opposite a heated vertical wall containing an array of two-dimensional rectangular rib elements and found that it improved the heat transfer characteristics in the duct and reduced the occurrence of hot spots. Myrum *et al.* [2] examined the effect of placing a vortex generator (circular rod) above or just downstream of a two-dimensional rib. It was found that the generator resulted in increases in the average Nusselt number as high as 30% at $Re = 3300$. Garimella and Eibeck [3] examined the effect of protruding vortex generators (half-delta wings placed at a 20° angle of attack to the flow) on the heat transfer from an array of discrete heated elements. A peak heat transfer enhancement of 40% occurred in the second row of elements. Measurements [4] of the turbulent heat transport in a boundary layer with a protruding generator demonstrated that the vortex interaction with the turbulent boundary layer enhanced the heat transport to a greater extent than the momentum transport. References [5–7] showed that for laminar flow, circular wires placed above a smooth horizontal surface resulted in a premature transition to turbulent flow conditions causing increased heat and mass transfer rates.

The main objective of the present investigation is to study the effect of vortex generators on the heat transfer, the pressure drop, and the thermodynamic irreversibilities (destruction of available work) in a ribbed duct. Local and average Nusselt number results, deduced from local wall temperature measurements, and overall pressure results were obtained for an air flow ($Re = 3450$) through an asymmetrically heated rectangular ribbed duct with vortex generators (circular rods) placed immediately above or just downstream of preselected rib elements. The performance of the various generator configurations are evaluated using dimensionless augmentation numbers: the augmentation Nusselt number, $N_{\overline{Nu},a}$, the augmentation Nusselt-friction-factor number, $N_{\overline{Nu}\bar{f},a}$, and the augmentation entropy-generation number, $N_{s,a}$. The augmentation entropy-generation number [8] is a thermodynamically based measure for evaluating heat transfer augmentation schemes and includes competing pressure drop irreversibilities and heat transfer irreversibilities. A reduction in $N_{s,a}$ indicates overall enhancement.

THE EXPERIMENTS

The experiments were conducted in an insulated asymmetrically heated test section which was located after a 40-hydraulic-diameter-long flow-development section. A constant heat flux was simulated along the bottom wall of the test-section by dissipating d.c. current in a 0.025-mm-thick stainless steel shim. Chromel–constantan thermocouples (0.076 mm dia.), spot welded to the under-side of the shim along the centerline, were used to measure the local shim temperatures. Thermocouples positioned at off-centerline locations confirmed that the spanwise temperature variation was within 0.1°C, which is the uncertainty of the temperature measurements. The maximum effect of the heating current on the measured thermocouple voltage was also less than 0.1°C. To minimize buoyancy effects, the power supplied to the shim was set to give $Gr_H/(Re_H)^2 < 0.10$, where Gr_H and Re_H are the duct height based Grashof and Reynolds numbers, respectively, and Gr_H is based on the maximum shim-to-inlet temperature difference.

NOMENCLATURE

A	cross-sectional area (186 ± 2 cm^2 [9])
c_p	constant pressure specific heat of air
d	diameter of the cylindrical vortex generator (Fig. 2)
D_h	hydraulic diameter (10.2 ± 0.1 cm [9])
$\bar{f}$	average friction factor $(2D_h(-\Delta p/L_1)\rho U^2)$ (uncertainty $[9] \pm 6.4\%$)
H	duct height (6.10 ± 0.06 cm)
h	rib height (6.35 mm)
k	air thermal conductivity at $(T_{b,in} + T_b(L_1))/2$
$k(x)$	air thermal conductivity at $(T_w(x) + T_b(x))/2$
L	downstream displacement of the rod from the rib centerline (Fig. 2)
L_1	heated length (99.8 ± 0.2 cm)
$\dot{m}$	mass flow rate (uncertainty $[9] \pm 2.0\%$)
$N_{\overline{Nu},a}$	augmentation Nusselt number $(\overline{Nu}_a/\overline{Nu}_0)$ (uncertainty $[9] \pm 3.5\%$)
$N_{\overline{Nu}\bar{f},a}$	augmentation Nusselt-friction-factor number $((\overline{Nu}/\bar{f})_a/(\overline{Nu}/\bar{f})_0)$ (uncertainty $[9] \pm 10\%$)
$N_{s,a}$	augmentation entropy-generation number (S'_a/S'_0) (uncertainty $[9] \pm 7.0\%$)
Nu	local Nusselt number $(q''_c(x)D_h/(T_w(x) - T_b(x))k(x))$ (uncertainty $[9] \pm 5.3\%$)
$\overline{Nu}$	average Nusselt number $((D_h/k)\int_0^{L_1} q''_c(x)\,dx/\int_0^{L_1}(T_w(x) - T_b(x))\,dx)$ (uncertainty $[9] \pm 2.5\%$)
P	rib pitch (Fig. 1)
q'_c	heat transfer per unit heated length $((w/L_1)\int_0^{L_1} q''_c(x)\,dx)$ (uncertainty $[9] \pm 2.1\%$)
$q''_c(x)$	convective heat flux corrected for radiation and conduction losses (uncertainty $[9] \pm 4.6\%$)
Re	Reynolds number (UD_h/ν) (uncertainty $[9] \pm 2.4\%$)
S'	entropy generation per unit heated length (equations (2) and (3)) (uncertainty $[9] \pm 5.0\%$)
s	rod–rib spacing
$T_b(x)$	local bulk temperature $((w/\dot{m}c_p)\int_0^x q''_c(x')\,dx' + T_{b,in})$ (maximum uncertainty $[9] \pm 0.16$°C)
$T_{b,in}$	measured inlet bulk temperature (measured to within ± 0.12°C)
$T_w(x)$	local shim temperature (measured to within ± 0.12°C)
t	intergenerator spacing, tandem configuration (Figs. 2(c) and (d))
U	average duct velocity $(\dot{m}/\rho A)$ (uncertainty $[9] \pm 2.2\%$)
w	channel width (30.5 ± 0.1 cm)
x	streamwise (axial) coordinate.

Greek symbols

Δp	average pressure change over the heated length (uncertainty $\pm 2.3 \times 10^{-5}$ mm Hg)
$\overline{\Delta T}$	average shim-to-bulk temperature difference $((1/L_1)\int_0^{L_1}(T_w(x) - T_b(x))\,dx)$
ν	kinematic viscosity at $(T_{b,in} + T_b(L_1))/2$.

Subscripts

a	augmented case (vortex generators)
0	baseline case (ribs only).

Local Nusselt number results for the heated wall of the test section were determined from the local convective heat flux, $q''_c(x)$, and the measured shim temperatures. The determination of $q''_c(x)$, involved subtracting local conduction and radiation heat losses from the local electric heat flux generation (measured to within 2.0%), which was determined from measurements of the current (measured to within 0.1%) supplied to the shim and the temperature-dependent electrical resistivity of the shim (measured to within 1.8%). A finite-difference procedure was used to compute the conduction heat losses to within 8%. Temperatures measured to within ± 0.12°C along the inner surfaces of the side walls and the top wall were used as boundary conditions in the heat conduction code and were the dominant sources of uncertainty in the conduction loss. Local radiation losses were estimated to within 15% [9] using $\varepsilon = 0.20 \pm 0.03$ for the shim and $\varepsilon = 0.9 \pm 0.1$ for the plexiglas top wall and side walls. The emissivity uncertainties were the dominant sources of uncertainty in the computed radiation loss. The conduction and radiation losses both ranged from 10 to 18% of the local electric heat flux generation.

Pressure drop measurements were performed using a differential pressure sensor with a resolution to 1.0×10^{-6} mm Hg and an accuracy of 0.05% of the reading. The pressure drop measurements were accomplished by connecting the two ports of the sensor to two pressure taps respectively located 1.0 mm upstream and downstream of the respective upstream and downstream edges of the heated shim. The uncertainty in the pressure drop measurement was $\pm 2.3 \times 10^{-5}$ mm Hg, which was 4.5% of the smallest pressure drop recorded.

Figure 1 displays the two rib distributions—referred to as Case I and Case II—of this study. For

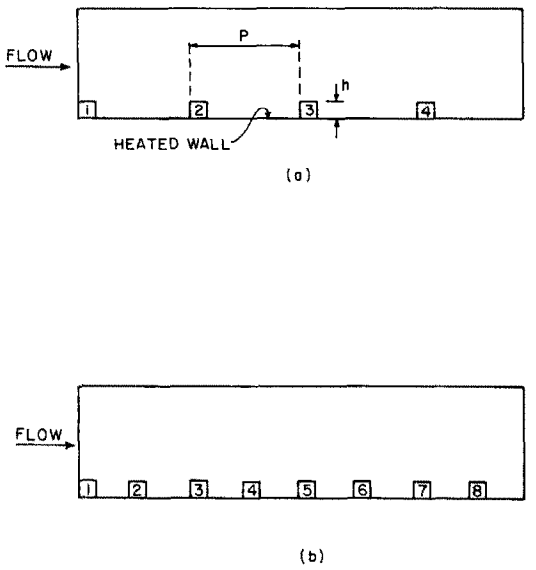

FIG. 1. Rib distributions: (a) Case I; (b) Case II.

both cases, two-dimensional, square, balsa-wood ribs were affixed to the heated shim surface using 0.025-mm-thick double-sided tape. The upstream face of the leading rib was flush with the beginning of the shim. As seen in the figure, Case I consisted of four ribs, deployed to give a dimensionless pitch of $P/h = 38.4$, while Case II consisted of eight ribs, deployed to give $P/h = 19.2$. The thermocouples discussed earlier were distributed to give a wall temperature measurement at 5.1 ± 0.1 mm increments in the first and seventh interrib spaces of Case II and every 10.2 ± 0.1 mm increments in the remaining interrib spaces. Four different generator configurations were studied (see Fig. 2): two single configurations and two tandem configurations.

EXPERIMENTAL RESULTS

Uncertainty, reproducibility, and preliminary results

Experimental uncertainties were computed using the method of Kline and McClintock [9]. For a result, $R = R(x_1, x_2, \ldots x_n)$, the uncertainty computed using this method is

$$u_R = \left\{ \sum_{i=1}^{n} [(\partial R/\partial x_i) u_i]^2 \right\}^{1/2} \quad (1)$$

where u_i is the uncertainty in the ith variable. The uncertainties of all the quantities presented in this paper are given in the Nomenclature, as are the uncertainties in the terms appearing in the defining equations for these quantities. Uncertainties computed from applying equation (1) to a defining relation are denoted by '[9]', whereas the uncertainty in any directly measured quantity (i.e. temperatures, dimensions, etc.) was deduced from the standard deviation for ten independent representative measurements of

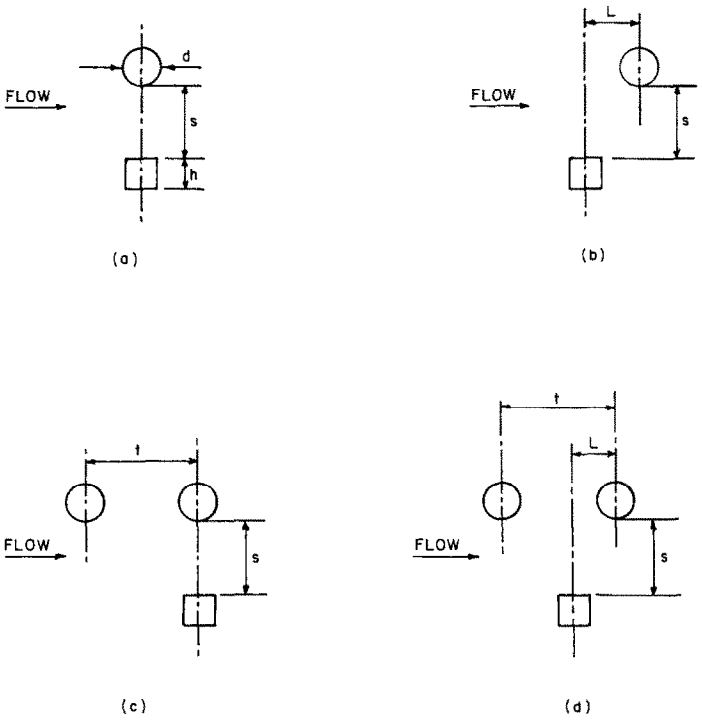

FIG. 2. Vortex generator configurations: (a) single in-line configuration; (b) single displaced configuration; (c) tandem in-line configuration; (d) tandem displaced configuration.

the quantity. Uncertainties in the local conduction loss were determined by computing the loss for variations in the measured boundary temperatures (± 0.12°C, the measurement uncertainty). The maximum deviation in the conduction loss, caused by varying the boundary temperatures, was 8% of the nominal conduction loss and was taken to be the uncertainty. Uncertainties in the thermophysical properties were determined to be negligible and are not included in the uncertainties reported in this paper. Of particular importance is the calculation of the uncertainties in the integrals. All of the integrals were approximated by summations, and the uncertainty was computed by applying equation (1) to each summation.

Reproducibility results are shown in Fig. 3 for the two baseline cases. The average Nusselt numbers for Cases I and II could be reproduced to within 4.6 and 2.7%, respectively. To test the experimental apparatus and the methods used to account for the heat conduction and radiation losses, a set of data runs was performed for a smooth duct. For a nominal Reynolds number of 3400, it was found that the average Nusselt number was within 2.2% of that predicted by the correlation of Gnielinski [10].

Local heat transfer results

As mentioned before, the baseline results for the two ribbed-duct cases are shown in Fig. 3. The solid squares on the abscissa denote the rib locations for the respective cases, and each data point corresponds to a thermocouple location. A local Nusselt number is also reported for the thermocouple locations immediately below each rib. These *Nu* values are computed as if the rib were not there and are included in the calculation of the average results. It is felt that these 'pseudo-*Nu*' values will in no way affect the comparisons about to be presented.

Inspection of the figure shows that for both cases, the location of the interrib maximum Nusselt number shifts upstream in going from the first interrib space to the second. This is caused by an upstream shift in the reattachment point, which occurs just downstream of the peak *Nu* location [11]. Liou *et al.* [12] and Durst *et al.* [13] both observed shorter reattachment lengths behind the second rib and reasoned it was due to the difference in the upstream flow conditions, relative to those upstream of the first rib. It is also seen that the interrib peak Nusselt number for Case I decays in the streamwise direction. In contrast, the interrib peak for Case II increases in going from the first to the second interrib space. The phenomenon is clearly induced by the comparatively close proximity of the second rib. Note further that the peak *Nu* value in the first interrib space for Case I lies downstream of that for Case II. Since both cases have virtually identical upstream flow conditions, the close proximity of the second rib in Case II has forced the flow to reattach prematurely.

Figure 4 demonstrates the effect of placing a single vortex generator directly above each of the four ribs of Case I at different distances (see Fig. 2(a)). The open symbols above the black squares on the abscissa of the graphs in this figure, as well as in the remaining

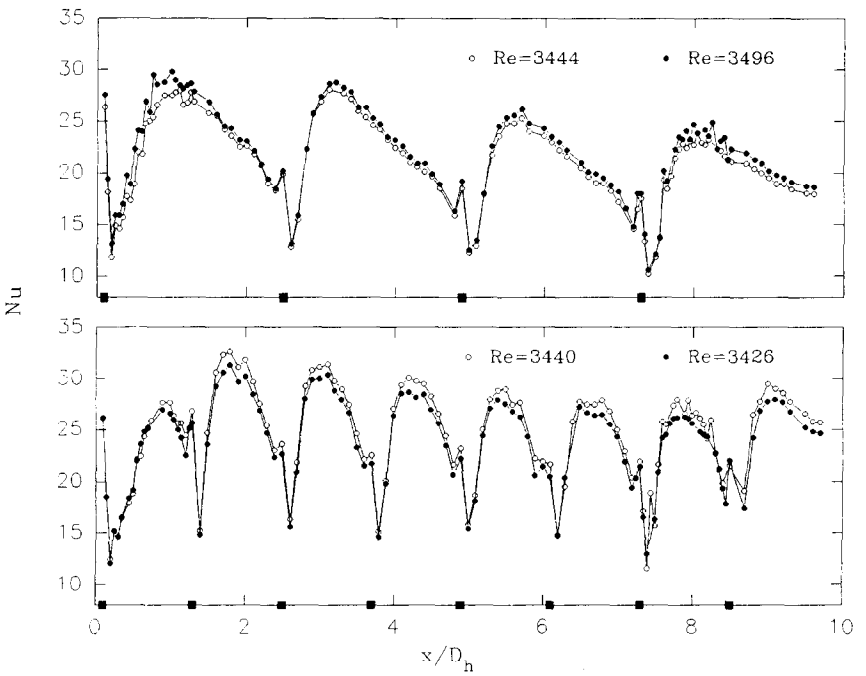

FIG. 3. Local Nusselt results for the rib-only baseline cases: Case I (top); Case II (bottom).

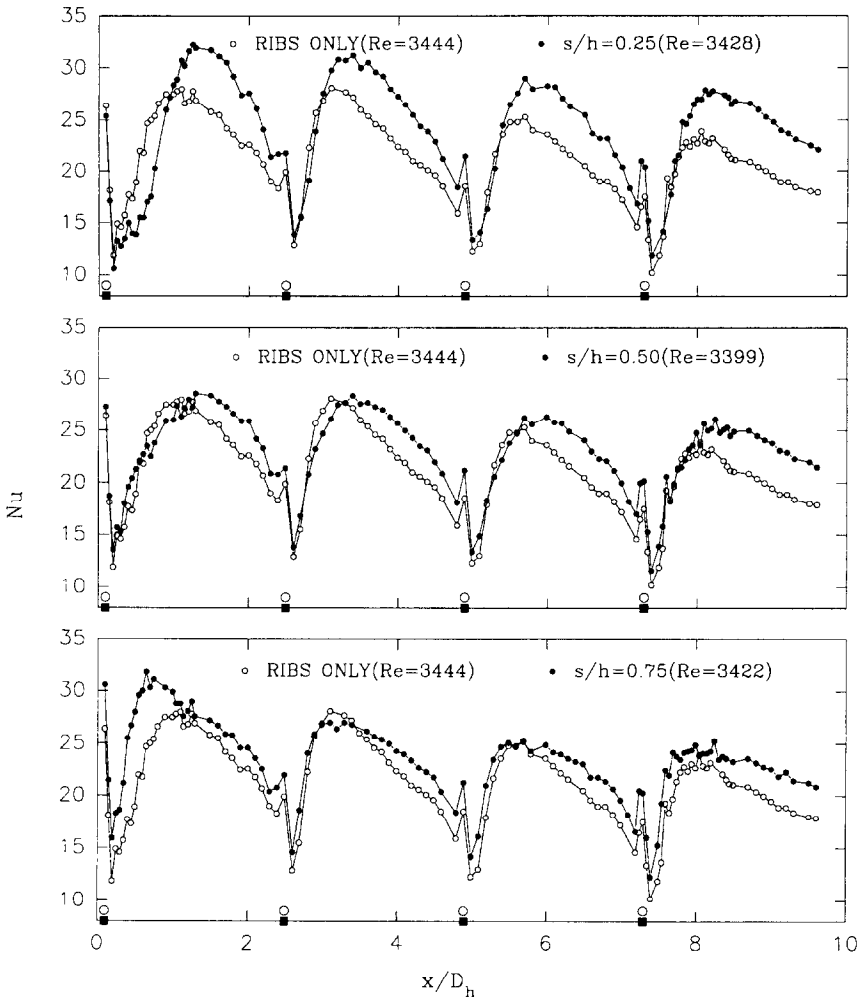

FIG. 4. Effect of the single in-line configuration on the local Nusselt results of Case I at different s/h values above ribs 1–4 for $d/h = 0.50$.

figures of this paper, depict the vortex generators. The open data symbols appearing on this figure and the rest of the figures in the paper denote the respective rib-only baseline cases and correspond to the open symbols of the graphs in Fig. 3.

Figure 4 shows that generators positioned at $s/h = 0.25$ above the ribs result in Nusselt number enhancement. It is also noticed that at the 0.25 and 0.50 spacings, the presence of the generator causes a downstream shift in all of the interrib peak Nu locations. For $s/h = 0.75$, the presence of the generator results in an upstream shift in the initial Nu peak only, with the remaining peak locations being unaffected.

For a flow past a single generator–rib element, Myrum *et al.* [2] attributed the upstream shift at $s/h = 0.25$ to the generator–rib pair acting as a single disturbance element, because the generator–rib space is so small. It is believed that the increase in the effective height promotes turbulence, which in turn enhances the Nusselt numbers. For $s/h = 0.50$, the decrease in the peak Nu values relative to those for $s/h = 0.25$ is believed to be caused by the fact that at $s/h = 0.50$, enough flow passes through the space to impact the near-wall flow field and thus the heat transfer. It is reasoned that although the flow impacts the heat transfer, it does so in a negative way—relative to the $s/h = 0.25$ case—because the friction in the space leads to a reduction in the local velocities and suppresses the turbulence.

At $s/h = 0.75$, an even larger share of the flow passes through the rib-generator space. As seen in the figure, this results in an upstream shift in the peak Nu location behind the leading rib. Myrum *et al.* [2] reasoned that at this spacing, the rib and the generator are essentially functioning as separate entities, and the reattachment length is determined to a large degree by the rib height. The fact that the initial peak lies upstream of that for the baseline is believed to be the

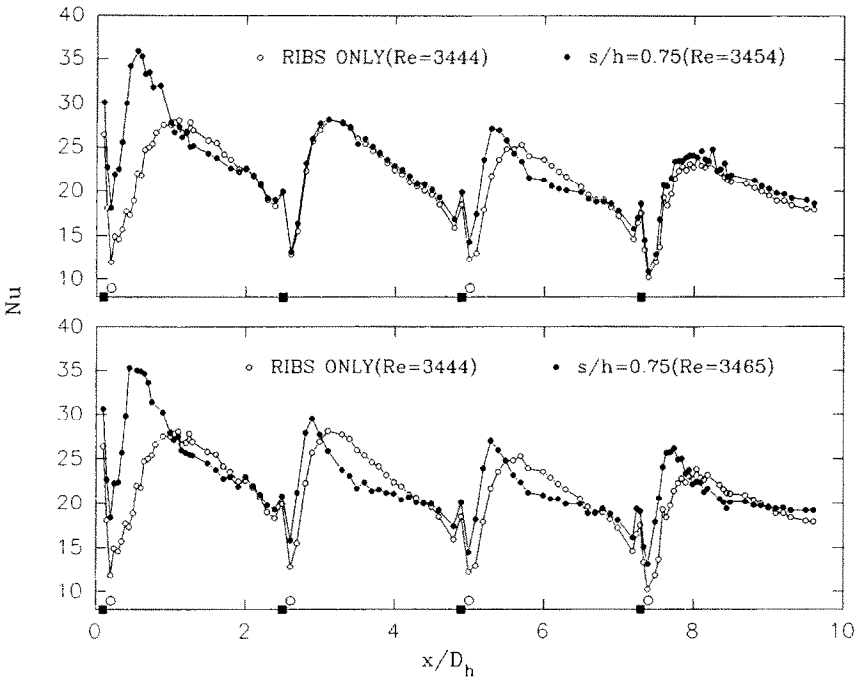

FIG. 5. Effect of the single displaced configuration ($L/h = 1.75$) on the local Nusselt results of Case I for different streamwise generator distributions for $d/h = 0.50$.

result of increased turbulence levels caused by the presence of the rod. This is also believed to be the cause of the increased *Nu* values.

The effect of moving the generators downstream of their adjacent ribs (Fig. 2(b)) is examined in Fig. 5 for $L/h = 1.75$ and $s/h = 0.75$. In contrast to the behaviour displayed for the single in-line configuration at $s/h = 0.75$ in the preceding figure, the peak *Nu* values migrate upstream in every interrib space where there is a generator. However, significant enhancement of the local Nusselt number occurs only in the first interrib space. Note, too, the peak is considerably higher than the corresponding peak for the single in-line setup. In the interrib spaces where there are no generators, the *Nu* data duplicate the baseline case. This demonstrates that the effect of each generator in this case is a localized one and is confined to the interrib space where the generator is located.

An upstream migration in the peak *Nu* was also observed by Myrum *et al.* [2] for a generator positioned just downstream of a single rib. It is believed that as the flow goes around the generator, the portion of the flow that passes underneath it alters the trajectory of the shear layer causing premature reattachment. The large degree of enhancement behind of the leading rib is most likely caused by the increased turbulence levels induced by the rod, while the diminished effect of the generators downstream is due to the belief that the turbulence levels are elevated to the point where further enhancement by the generators is no longer possible.

Results for eight ribs (Case II, Fig. 1(b)) are displayed in Fig. 6 for the single in-line generator configuration. Similar to the results presented in Fig. 4 for Case I, the presence of the generator at $s/h = 0.25$ causes a downstream shift in the peak *Nu* locations in the interrib spaces immediately behind the generators. At $s/h = 0.75$, an upstream shift is observed behind the first generator and no shift is observed behind the second generator located above the fifth rib. Recall that the rib and generator act as separate entities at $s/h = 0.75$.

For $s/h = 0.25$, the effect of the generator is also manifested in increased *Nu* values and upstream shifts in the peak *Nu* locations in the interrib spaces downstream of the ribs with no generators, with these effects diminishing in the streamwise direction. Downstream of the second rib, this effect persists for two interrib spaces, whereas downstream of the sixth rib, this effect is observed only in the first downstream space. The fact that the peak *Nu* values in the interrib spaces immediately behind the generators occur near the downstream rib suggests that the flow reattachment points are quite close to the downstream ribs and thus the recirculation region spans nearly the entire interrib space. Consequently, the local Nusselt numbers are lower than those for the baseline over a substantial portion of the interrib space. Since the reattachment points behind the generator–rib pairs are so close to the downstream rib, it is believed that the increased *Nu* values and the upstream shift in the peak *Nu* location behind these ribs are caused by the high turbulence levels associated with reattachment.

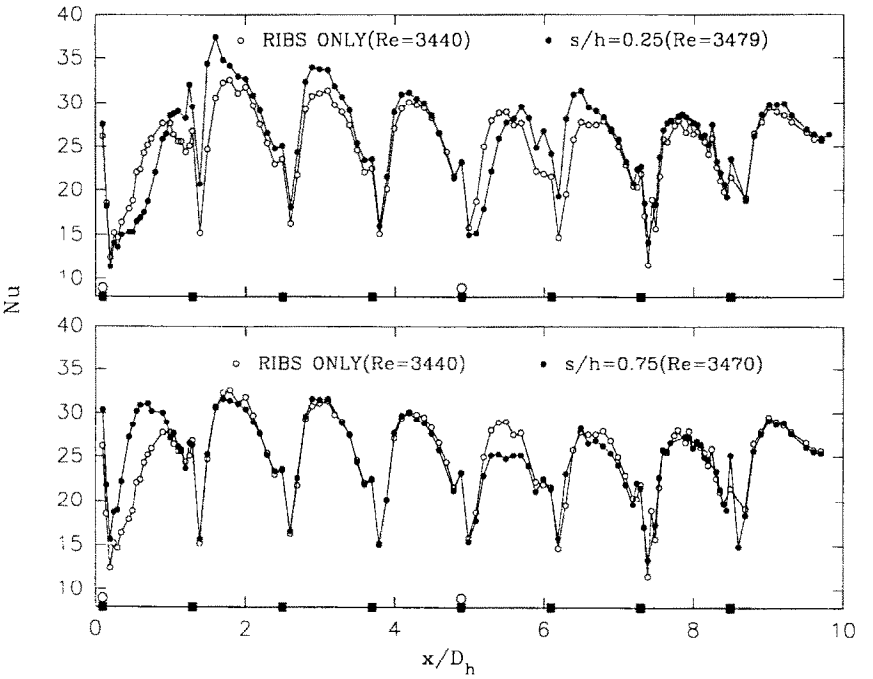

FIG. 6. Effect of the single in-line configuration on the local Nusselt results of Case II at the different s/h values above ribs 1 and 5 for $d/h = 0.50$.

The behavior at $s/h = 0.75$ lends credence to the reasoning behind the trends described for $s/h = 0.25$. It is seen that the reattachment point in the initial interrib space lies upstream of that for the baseline and well upstream of that for $s/h = 0.25$. Since the turbulence levels decay downstream of reattachment, the turbulence levels at the second rib are lower than those for $s/h = 0.25$. Consequently, the Nu results in the second interrib space are the same as those for the baseline. It is interesting to note that the presence of the second generator for $s/h = 0.75$ degrades the Nusselt number.

Figures 7 and 8 examine the effects of the generator spacing and different generator distributions for the single in-line generator configuration with $d/h = 1.0$, which represents a doubling of the generator diameter. A comparison of the results in the bottom graph of Fig. 6 with those at the top of Fig. 7 reveals that the maximum Nu location behind the leading generator does not migrate upstream as it did for $d/h = 0.50$ and $s/h = 0.75$. Therefore, since the reattachment point is closer to the second rib, the Nu peak in the adjacent downstream interrib space, where there is no generator, is enhanced and migrates upstream in much the same way as it did for $s/h = 0.25$ in Fig. 6. In the interrib regions immediately behind the downstream generators, the generator either degrades the local Nu as it did for $d/h = 0.50$ or leaves it virtually unchanged.

An inspection of Fig. 7 together with the middle graph in Fig. 8 shows that immediately behind the generators, the interrib peaks increase with increasing s/h. Interestingly, there is a decrease in Nu in the interrib regions downstream of the ribs without the generators, except in the first such region for $s/h = 1.0$. It is also observed that the interrib peak Nu locations behind the generators move upstream with increasing s/h. This was observed for Case I for $d/h = 0.50$ and was attributed to the rib and the generator becoming independent of each other.

Figure 8, by itself, examines the effect of three different streamwise generator distributions for $s/h = 1.50$. As in the preceding figures, the generator-induced enhancement is confined mainly to the interrib region behind the first generator. The degradation observed downstream for the multiple generator configurations demonstrates that the lone generator configuration (top graph) performs the best.

Results for the tandem in-line generator configuration (Fig. 2(c)) are displayed in Fig. 9. The use of the tandem configuration was motivated by the fact that the vortex shedding frequency behind the tandem pair depends on the intergenerator spacing, t, (Zdravkovich [14]) and that the frequency behind the pair is different from that behind a single generator. The figure shows that the tandem pair degrades the local interrib Nusselt numbers in the first interrib space for $s/h = 0.25$ and 0.50, while modest enhancement occurs at $s/h = 0.75$. At all spacings, the presence of the tandem pair over the leading rib leads to a reduction in the Nu values in the second interrib space.

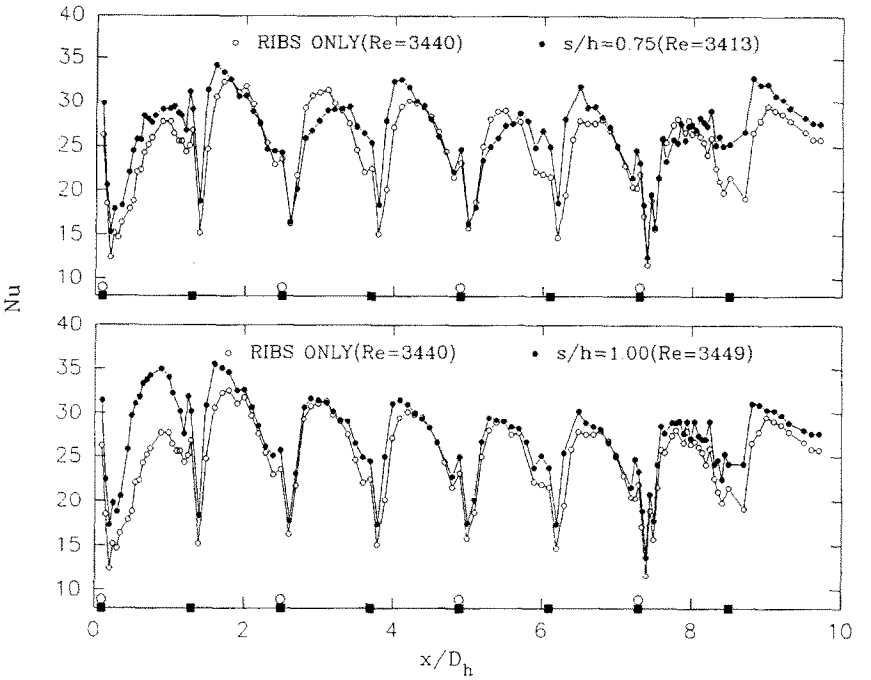

FIG. 7. Effect of the single in-line configuration on the local Nusselt results of Case II at different s/h values above ribs 1, 3, 5, and 7 for $d/h = 1.0$.

A comparison of the top graph to that for the single generator configuration in Fig. 6 shows that the tandem pair results in a greater downstream shift, for $s/h = 0.25$, in the first interrib Nu distribution and lower interrib Nu values. Increasing s/h to 0.50 causes the Nu peak to move upstream because the generator and the rib start to function independently at the larger spacings. In keeping with previous results, the upstream movement of the reattachment point causes a decrease in the Nu values in the next interrib space.

For $s/h = 0.75$, the reattachment-induced Nu peak is much larger than at $s/h = 0.50$, with the $s/h = 0.75$ peak occurring at the same interrib location as that for $s/h = 0.50$. It is also observed that the valley in the interrib distribution observed for $s/h = 0.50$ has disappeared. The depressed Nu values at $s/h = 0.50$ are probably due to a reduction in the local velocities because of the higher friction associated with the smaller interrib space.

Comparing the $s/h = 0.75$ results to those for the single configuration at the bottom of Fig. 6 shows that the two Nu distributions in the first interrib space have the same shape. A closer inspection of the two figures reveals that the single generator results in greater Nu enhancement behind in the first interrib space as well as higher Nu values in the adjacent interrib space. This is believed to be caused by the greater friction associated with the additional rod for the tandem pair.

Results for the tandem displaced configuration (Fig. 2(d)) are shown in Fig. 10. A comparison of the results to the tandem-in-line results at the top of Fig. 9 and the single-in-line results at the top of Fig. 6 reveals that the results are more like the single-in-line results than the tandem-in-line results of Fig. 9. That is, the downstream shift in the tandem pair results in a slight upstream shift in the Nu peak in the first interrib space and Nu augmentation in the second interrib space. A comparison of the results in the interrib space behind the second generator configuration, located downstream, along with the results in the adjacent downstream interrib space in Fig. 10 with the corresponding results in Fig. 6 shows that the tandem pair degrades Nu to a larger extent in the interrib region immediately behind the generator and retards the Nu recovery in the adjacent interrib space. This again can be attributed to a reduction in the local velocities caused by the friction introduced by the additional rod.

Average results

Average results are displayed in Table 1. Reading from the left, the second column gives the various generator configurations by listing the figure number in which they appear, while the third column lists the numbers of the ribs adjacent to the generator configuration (see Fig. 2) and thereby gives the number of generator configurations and their locations.

The average results are presented in the last three columns at the right and are respectively from left to right : the augmentation Nusselt number, $(N_{\overline{Nu},a} (= \overline{Nu}_a/\overline{Nu}_o)$, the augmentation Nusselt-

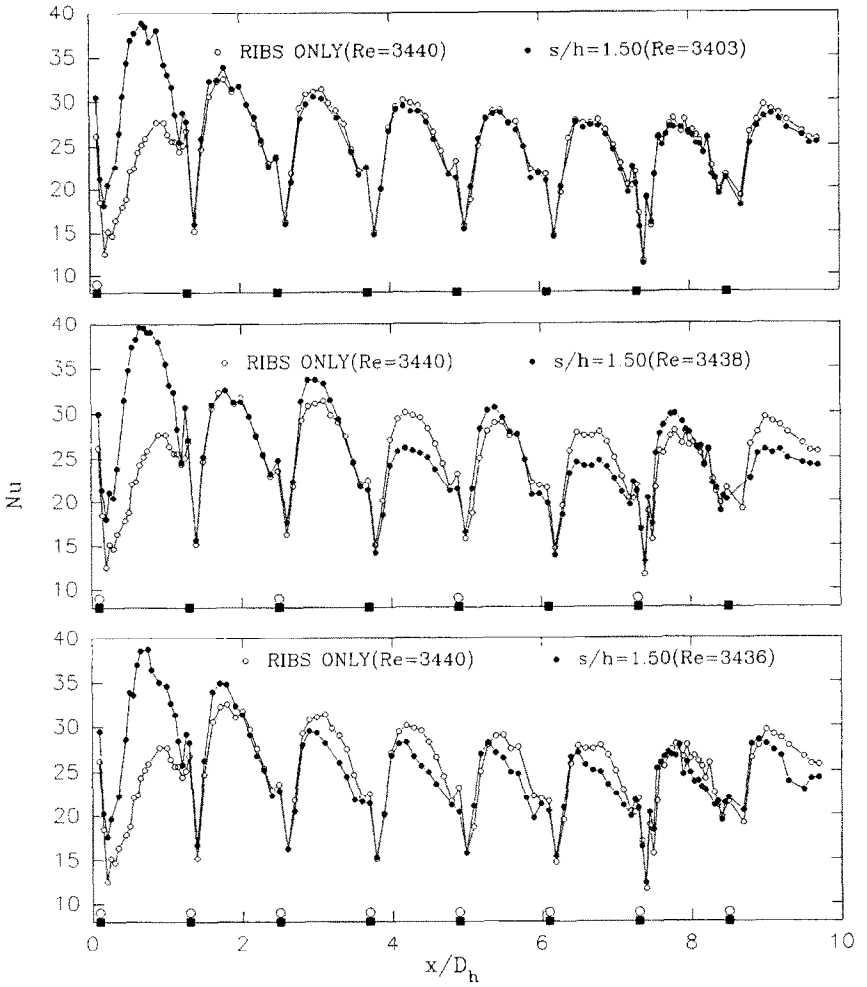

FIG. 8. Effect of the streamwise distribution of the single in-line configuration on the local Nusselt results of Case II for $d/h = 1.0$.

friction-factor number, $N_{\overline{Nu}/\bar{f},a}(=(\overline{Nu}/\bar{f})_a/(\overline{Nu}/\bar{f})_o)$, and the augmentation entropy-generation number [8], $N_{s,a}(=S'_a/S'_o)$, where S' is the entropy generation per unit heated length. In this notation, the subscript 'a' refers to the augmented case, and the subscript 'o' refers to the baseline case.

The augmentation entropy-generation number is due to ref. [8] and is a measure of the ability or inability of an augmentation technique to conserve useful work (exergy). The augmentation entropy-generation number is determined by computing S' for both the augmented and baseline cases using ref. [8]

$$S' = \frac{\dot{m}}{\rho T^*}\left[-\frac{\Delta p}{L_1}\right] + \frac{q'_c\overline{\Delta T}}{T^{*2}} \tag{2}$$

where T^*, $(-\Delta p/L_1)$, q'_c, and $\overline{\Delta T}$ are the absolute temperature, set equal to the inlet bulk temperature, $T_{b,in}$, the average measured pressure drop per unit heated length, the heat transfer per unit heated length, and the wall-to-bulk temperature difference averaged over L_1, respectively. It should be mentioned that $(-\Delta p/L_1)$ is used in place of $(-\mathrm{d}p/\mathrm{d}x)$ in the original equation of ref. [8]. Substituting the relations for q'_c and $\overline{\Delta T}$ into (2) and using $\overline{Nu}$ gives

$$S' = \frac{\dot{m}}{\rho T^*}\left(-\frac{\Delta p}{L_1}\right) + \frac{(q'_c)^2 D_h}{wT^{*2}k\overline{Nu}}. \tag{3}$$

In equations (2) and (3), the first term on the right is the fluid-flow irreversibility, and the second term is the heat-transfer irreversibility. Bejan [8] formed the ratio of these two terms for the baseline case to get the baseline irreversibility distribution ratio

$$\phi_0 = \left(\frac{\dot{m}}{\rho T^*}\left(-\frac{\Delta p}{L_1}\right)\right)_o \Big/ \left(\frac{(q'_c)^2 D_h}{wT^{*2}k\overline{Nu}}\right)_o. \tag{4}$$

For Case I and Case II, $\phi_0 = 0.0020$ and 0.0035, respectively. Therefore, the heat-transfer irreversibility totally dominates. Bejan and Pfister [15] found that

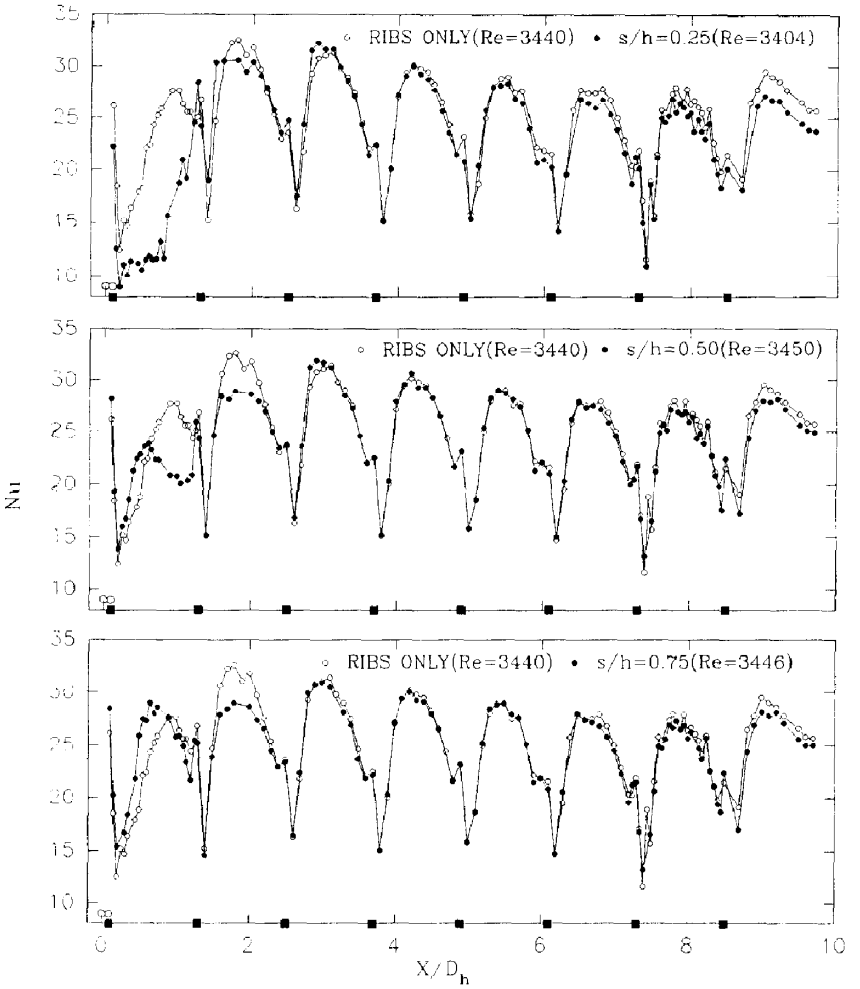

FIG. 9. Effect of the tandem in-line configuration ($t/h = 1.5$) on the local Nusselt results of Case II at different s/h values above the first rib for $d/h = 0.50$.

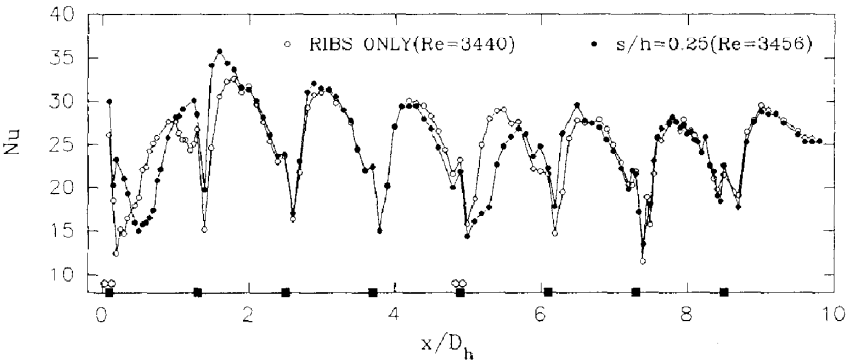

FIG. 10. Effect of the tandem displaced configuration ($t/h = 1.5$, $L/h = 0.5$) placed over ribs 1 and 5 on the local Nusselt results of Case II for $d/h = 0.50$.

Table 1. Average results

P/h (Fig. 1)	Config. Fig. no.	Gen. loc. Rib nos.	t/h	L/h	d/h	s/h	$N_{\overline{Nu},a}$	$N_{\overline{Nu}f,a}$	$N_{s,a}$
38.4	2a	1, 3	NA	0	0.50	0.25	1.07	0.77	0.94
						0.50	1.07	0.70	0.93
						0.75	1.05	0.79	0.95
38.4	2a	1, 2, 3, 4	NA	0	0.50	0.25	1.10	0.57	0.91
						0.50	1.08	0.56	0.93
						0.75	1.09	0.54	0.92
38.4	2a	1, 2, 3, 4	NA	0	1.0	1.0	1.21	0.40	0.83
						1.5	1.19	0.40	0.85
38.4	2b	1,2	NA	1.75	0.50	0.75	1.03	0.91	0.97
		1, 2, 3, 4					1.03	0.63	0.97
38.4	2d	1, 3	1.5	0.50	0.50	0.25	1.09	0.73	0.92
19.2	2a	1, 5	NA	0	0.50	0.25	1.05	0.96	0.96
						0.75	1.03	0.82	0.98
19.2	2a	1	NA	0	1.0	1.0	1.10	0.76	0.92
						1.5	1.05	0.95	0.96
19.2	2a	1, 3, 5, 7	NA	0	1.0	0.75	1.09	0.56	0.93
						1.0	1.12	0.56	0.91
						1.5	1.04	0.57	0.97
19.2	2a	1–8	NA	0	1.0	1.5	1.03	0.45	0.98
19.2	2c	1	1.0	0	0.50	0.50	1.05	0.84	0.92
19.2	2c	1	1.5	0	0.50	0.25	0.94	0.76	1.07
						0.50	1.00	0.86	1.00
						0.75	1.01	0.80	0.99
19.2	2d	1	1.5	0.50	0.50	0.25	1.03	0.94	0.98
						0.50	1.03	0.82	0.97
19.2	2d	1, 5	1.5	0.50	0.50	0.25	1.02	0.68	0.99

a marginal value of ϕ_0 exists which is typically less than one. When ϕ_0 is less than the marginal value, the entropy generation can be decreased by using a heat transfer augmentation scheme. If the value is exceeded, then the entropy generation will be increased by using an augmentation scheme, even though the heat transfer is enhanced. Incidently, the ϕ_0 value for the smooth duct is 0.0009.

Before discussing Table 1 in detail, it should be mentioned that in computing the augmentation numbers, the baseline values for each case were determined from the arithmetic averages of the average results for the two data sets of the corresponding case in Fig. 4. To ensure that $N_{s,a}$ only reflected the changes due to the augmentation schemes, the experiments were all performed for the same laboratory conditions, the same mass flow rates (maximum deviation 1.5%), and the same input power to keep q_c'' fixed within 1.0%.

Table 1 shows for Case I ($P/h = 38.4$) that the best performance occurs when the largest diameter generator ($d/h = 1.0$) is placed directly above every rib at $s/h = 1.0$ and 1.5. Here, $N_{\overline{Nu},a}$ attains its maximum values of 1.19 and 1.21 for $s/h = 1.5$ and 1.0, respectively, and $N_{s,a}$ attains is minimum values of 0.83 and 0.85 for $s/h = 1.0$ and 1.5, respectively. Incidently, $N_{\overline{Nu}f}$ attains its minimum values for this setup. However, the augmentation entropy-generation values indicate that it is the heat-transfer irreversibility that poses the larger threat. This is reflected in the fact that the irreversibility distribution ratio, ϕ_0, was only 0.0020. It is also seen for Case I that for a number of configurations, the presence of the generators have a negligible effect on the entropy generation, in that the entropy generation is close to or within its 5.0% uncertainty. Moreover, the average Nusselt number remains close to its 2.5% uncertainty for the single displaced configuration with small diameter ($d/h = 0.50$) generators.

Before turning to the tabulated results for Case II, it is of interest to examine the effect of decreasing the rib pitch in Case I ($P/h = 38.4$) to that of Case II ($P/h = 19.2$) on $N_{\overline{Nu},a}$ and $N_{s,a}$. In this comparison, Case II will play the role of the augmented case and Case I will remain as the baseline case. It is found that decreasing the rib pitch increases the average Nusselt number by 14% and decreases the entropy generation by 12%, and thus, the performance is better than all of the generator cases, except that where the largest diameter generators are placed above all four ribs.

An overview of the results for Case II tells immediately that the generators are not as effective for Case II as Case I. In fact, it is seen that for all but a few cases, the presence of the generators result in S' and $\overline{Nu}$ values that are within their respective uncertainties, indicating negligible enhancement. However, as in Case I, the best performance occurs for the largest diameter rod, with a 12% increase in the average Nusselt number and a 9% decrease in the entropy generation for rods placed directly above alternate ribs at $s/h = 1.0$. Noteworthy is the 10% increase in $\overline{Nu}$ and the 8% decrease in S' for a single large diameter generator placed over the first rib at $s/h = 1.0$.

As expected, from the discussion of the local results, the tandem generators performed rather poorly. The

notable exception occurs for the tandem displaced configuration placed at $s/h = 0.25$ above ribs 1 and 3 for Case I. Here it is seen that S' decreases by 8% and Nu increases by 9%.

Finally, it is interesting to compare the rib-only baseline of Case II to a smooth duct. It is found that the Case II ribbing results in a 73% increase in $\overline{Nu}$, a 28% decrease in $\overline{Nu}/\overline{f}$, and 42% decrease in S'. Note that even here, as in all of the cases considered, $Nu/\overline{f}$ decreases. However, the ϕ_0 value of 0.0009 given for the smooth duct indicates that the heat transfer irreversibility totally dominates and that a heat transfer augmentation scheme is advantageous. This fact is brought out by the decrease in S'. Clearly, the ribs reduced the heat transfer irreversibility to a much larger degree than they enhanced the pressure drop irreversibility, demonstrating the utility of the augmentation entropy-generation number for evaluating heat transfer augmentation schemes.

CONCLUDING REMARKS

Local and average Nusselt number and overall pressure drop results were determined experimentally for an air flow through a ribbed duct with vortex generators placed immediately above or just downstream of select rib elements. The effect of the various generator configurations were evaluated on an average basis by comparing the average Nusselt number, $\overline{Nu}$, the average Nusselt-friction-factor ratio, $\overline{Nu}/\overline{f}$, and the entropy generation per unit heated length, S', for the respective rib-only baseline cases to those for the generator cases. Comparisons of the local Nusselt number plots provided additional insights into the effect of the various generator configurations.

It was found that the generators had a larger impact on the heat transfer performance for a dimensionless rib pitch of $P/h = 38.4$ than for $P/h = 19.2$. At the larger pitch, the best performance resulted from placing the largest diameter generators ($d/h = 1.0$) directly over every rib, with the resulting effect corresponding to a 21% increase in $\overline{Nu}$ and a 27% decrease in S', while the best generator-induced performance at $P/h = 19.2$ (12% increase in $\overline{Nu}$, 9% increase in S') resulted from placing the largest diameter generator directly over every other rib. In addition, the results generally showed that the smaller diameter generators ($d/h = 0.5$) had a negligible effect on $\overline{Nu}$ and S'. The local Nusselt number results revealed that in all of the cases studied, generator-induced local Nu enhancement nearly always occurred in the interrib space behind the leading generator-rib pair, regardless of generator diameter. Downstream, the generators resulted in modest Nu enhancement at best and often times resulted in local Nu degradation.

Acknowledgement—This research was supported by the Gas Research Institute under Contract number GRI 5090-260-1961. Their support is gratefully acknowledged.

REFERENCES

1. Y. H. Hung and H. H. Lin, An effective installation of turbulence promotors for heat transfer augmentation in a vertical rib-heated channel, *Int. J. Heat Mass Transfer* **35,** 29–42 (1992).
2. T. A. Myrum, S. Acharya, S. Inamdar and A. Mehrotra, Vortex generator induced heat transfer augmentation in a heated duct air flow, *J. Heat Transfer* **114,** 280–284 (1992).
3. S. V. Garimella and P. A. Eibeck, Enhancement of single phase convective heat transfer from protruding elements using vortex generators, *Int. J. Heat Mass Transfer* **34,** 2431–2433 (1991).
4. D. E. Wroblewski and P. A. Eibeck, Measurements of the turbulent heat transport in a boundary layer with an embedded streamwise vortex, *Int. J. Heat Mass Transfer* **34,** 1617–1631 (1991).
5. D. G. Thomas, Forced convection mass transfer: Part II. Effect of wires located near the edge of the laminar boundary layer on the rate of forced convection from a flat plate, *A.I.Ch.E. Jl* **11,** 848–852 (1965).
6. D. G. Thomas, Forced convection mass transfer: Part III. Increased mass transfer from a flat plate caused by the wake from cylinders located near the edge of the boundary layer, *A.I.Ch.E. Jl* **12,** 124–130 (1966).
7. G. E. Kariadakis, B. B. Mikic and A. T. Patera, Minimum-dissipation transport enhancement by flow destabilization: Reynolds analogy revisited, *J. Fluid Mech.* **192,** 365–391 (1988).
8. A. Bejan, *Advanced Engineering Thermodynamics*. Wiley, New York (1988).
9. S. J. Kline and F. A. McClintock, Estimating uncertainty in single-sample experiments, *Mech. Engng* **75,** 3–8 (1953).
10. V. Gnielinski, New equations for heat and mass transfer in turbulent pipe and channel flow, *Int. J. Chem. Engng* **16,** 353–368 (1976).
11. T. M. Liou and J. J. Hwang, Turbulent heat transfer augmentation and friction in periodic fully developed channel flows, *J. Heat Transfer* **114,** 56–64 (1992).
12. T. M. Liou, Y. Chang and D. W. Hwang, Experimental and computational study of turbulent flows in a channel with two pairs of turbulence promoters in tandem, *J. Fluid Engng* **112,** 302–310 (1990).
13. F. Durst, M. Founti and S. Obi, Experimental and computational investigation of the two-dimensional channel flow over two fences in tandem, *J. Fluid Engng* **110,** 48–54 (1988).
14. M. M. Zdravkovich, Review—Review of flow interference between two circular cylinders in various arrangements, *J. Fluid Engng* **99,** 618–633 (1977).
15. A. Bejan and P. A. Pfister, Jr., Evaluation of heat transfer augmentation techniques based on their impact on entropy generation, *Lett. Heat Mass Transfer* **7,** 97–106 (1980).